Electrophoresis of a Biocolloid Covered with a Cation-Absorptive Membrane

Yung-Chih Kuo*

Department of Chemical Engineering, National Chung Cheng University, Chia-Yi, Taiwan 62102, Republic of China

Received: March 4, 2005; In Final Form: April 14, 2005

The electrophoretic behavior of a biocolloid covered with a charged membrane is theoretically analyzed in the present study. Here, the influences of nonuniformly distributed fixed groups, absorption of cations by fixed original functional groups, variation in dielectric constant in the electrophoretic system, and ionic sizes are considered. The results of numerical simulation suggest that a larger absolute value of the electrophoric mobility of biocolloids could be generated by larger membrane electricity. The absolute value of the electrophoric mobility for the nonlinear distribution of the fixed groups is larger than that for the linear distribution of the fixed groups. The absolute value of the electrophoric mobility increases with (1) the concentration of total fixed groups, (2) the cation-absorption equilibrium constant, (3) the nonuniform feature index for functional-groups distribution, (4) the dielectric constants of the inner uncharged membrane zone for only mobile cationic charge and for both mobile cationic and anionic charge, and (5) the effective size of the cations. An increase in the absolute value of the electrophoric mobility can also be resulted from a decrease in the following parameters: (1) the friction coefficient of the biocolloidal membrane phase, (2) the membrane thickness, (3) the dielectric constant of space for all charge and of outer uncharged membrane zone, (4) the effective sizes of anions and fixed groups, and (5) the number of cations and the fixed original functional groups involved in the formation of a cation-functional group complex.

1. Introduction

Electrophoresis is one of the most important modern techniques in chemical, biochemical and medical analyses for physiochemical properties of colloidal particles. The widespread applications of electrophoresis to natural or synthetic colloids include separation and purification of proteins and serums and determination of structural and interfacial characteristics of surfactants, dyestuffs, drugs, amino acids, nucleic acids, viruses and biological cells. In research on the surface properties of *Escherichia* coli and *Staphylococcus aureus* by electrophoresis, the electrostatic potential of the bacterial surface layer was observed to be appreciably influenced by the pH value and the ionic strength of the medium.[1] Furthermore, in a study of the electrophoresis of rat dorsal root ganglion neurons, the pH value and concentration of calcium ions of the medium were concluded to cause significant effects on the membrane charge and the electrophoretic mobility of the mammalian cells.[2] By employing an electrophoretic approach, the ultrastructure of human erythrocyte was also examined.[3] Moreover, applying the capillary zone electrophoresis to determine the amount of insulin in single cell was presumed to be beneficial to the fundamental understandings of diabetes and to the developments in clinical strategy for diabetic treatment.[4] From an experimental investigation on biological entities, the existence of an ion-penetrable layer, within which fixed charge is distributed, was confirmed.[5]

In the history of theoretical works on the electrophoresis of colloids, Smoluchoski[6] first developed the relation between the zeta potential and the electrophoretic mobility by assuming a constant electrostatic potential on the particulate surface. For a planar biocolloid covered by an ion-penetrable membrane, over which a fixed charge is uniformly distributed, the electrophoretic behavior of human erythrocytes was modeled through a linearized Poisson−Boltzmann equation, and analytic expressions for the distributions of the electrostatic potential and the fluid velocity were obtained.[7] It was concluded that the absolute value of the electrophoretic mobility of a particle possessing a peripheral membrane phase is smaller than that of the Smoluchoski formula. In addition, a modified version of the biocolloidal membrane was proposed by taking the concentration of fixed charge and the friction coefficient of the membrane phase into account, and a relatively simple expression for the electrophoretic mobility was derived.[8] Since various types of fixed charges exist in real cellular membranes, the critical traits of a biological cell can be dramatically affected by the distributions of a fixed charge. It was observed that the electrostatic effect of a nonuniform distribution of a fixed charge is stronger than that of a uniform one.[9−11] Furthermore, the nonuniformity of a fixed charge has a key effect on the double-layer properties[12] and on the interaction force and energy between two charged biocolloids.[13] The nonuniformity of a fixed charge was also found to yield a considerable influence on the electrophoretic mobility.[14] In addition, the electrophoretic behavior of biocolloids was examined by considering the effect of charge regulation, which reflects the degree of proton dissociation from the functional groups and improves the aspect of the fixed-charge distribution in the membrane phase.[15]

Although the above literature provides sufficient descriptions and explanations for the electrostatic behavior of biocolloids covered with a charged membrane, the sizes of ionic species are entirely neglected in these studies. In fact, ionic size plays a crucial role in the electrostatic characteristics of biocolloids, which was intensively discussed in a membrane-version modified Göuy-Chapman theory (MVMGCT).[16−19] Latterly, this

* To whom correspondence should be addressed. Tel: 886-5-2720411 ext. 33459. Fax: 886-5-2721206. E-mail: chmyck@ccu.edu.tw.

10.1021/jp051128b CCC: $30.25
Published on Web 05/18/2005

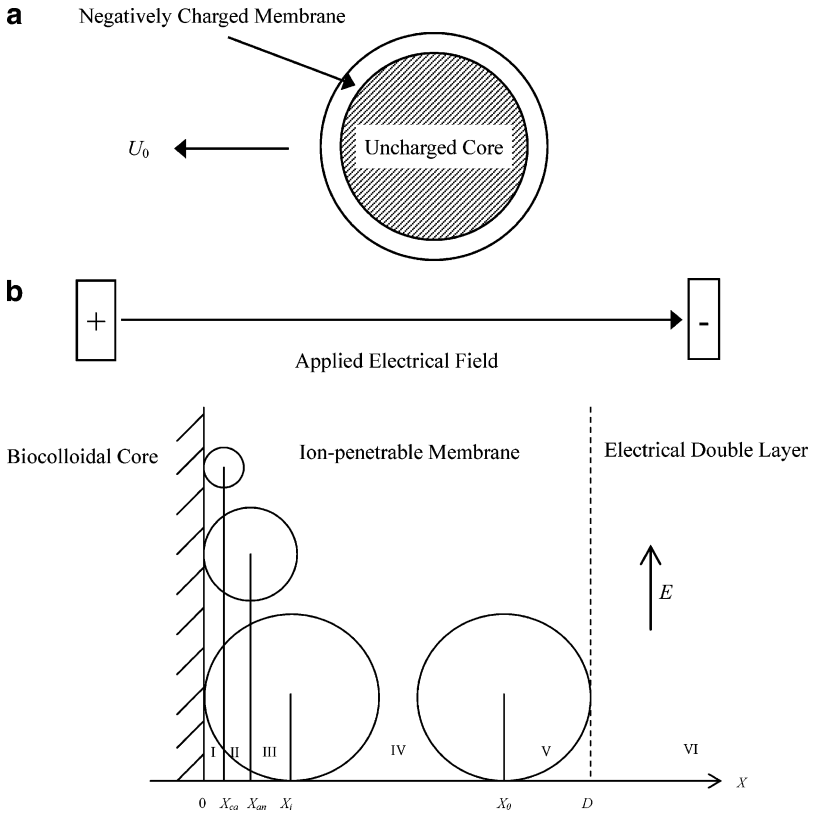

Figure 1. (a) Schematic representation of a negatively charged biocolloid under the influence of an applied electrical field. (b) Schematic representation of the electrophoretic system under consideration, where sizes of charged species are included by dividing the system into 6 regions with different charged species and/or dielectric constants.

theory was examined extensively for its applicability and validity in the interpretation of the influences of ionic sizes on the relevant biocolloidal behavior.[20−23] Nevertheless, the uptake of electrolyte species in the biocolloidal membrane was still ignored in the MVMGCT even if cellular incorporation of metallic ions occurs naturally in organisms and causes either growth stimulation or biological degeneration. Binding of divalent calcium within the peripheral regions of leukocytes and erythrocytes, for example, leads to a reduced electrostatic potential of those blood cells.[24] Hence, along with the effect of ionic sizes, a theoretical model for the absorption of cations in the external membrane layer was proposed for reflecting a more realistic behavior of biocolloids.[25] Besides, when contacting a rigid surface, the solvated layer structure of water molecules alters the dielectric constant, which is smaller for a space closer to the surface,[26] and distinguishable regions of the dielectric constant are present in the vicinity of an interface.[27] In an electrolyte solution, the appearance of ionic species also affects the dielectric properties of the charged membrane.[28] In the present study, the MVMGCT with the feature of cationic absorption in the exterior membrane layer is employed to investigate the electrophoretic behavior of biocolloids. Nonuniform distributions of the negatively charged functional groups and variations in the dielectric constant in the biocolloidal membrane are also considered. The effects of the friction coefficient of the biocolloidal membrane phase, membrane thickness, functional-groups concentration, nonuniform distribution of functional groups, cation-absorption equilibrium constant, numbers of cations and functional groups involved in the formation of a cation-functional group complex, effective sizes of cations, anions and functional groups, and dielectric constant on the electrophoretic mobility are especially studied.

2. Analysis

In the present study, electrophoresis of a biocolloid comprising an uncharged particulate core and a peripheral charged membrane of thickness d under the influence of an external electrical field of constant strength E is considered. Let the electrophoretic velocity of the biocolloid immersed in an a:b electrolyte solution be U_0. A schematic illustration of the electrophoresis of a negatively charged biocolloid under an applied electrical field is displayed in Figure 1a. Biocolloids can be regarded as planar particles because the majority of biocolloidal particles such as mammalian cells or protein molecules are much larger than their surrounding electrical double layers. Figure 1b shows a schematic representation of the electrophoretic system under consideration. Here, the scaled distance parameters are defined below.

$$X_{ca} = \kappa r_{ca} \tag{1a}$$

$$X_{an} = \kappa r_{an} \tag{1b}$$

$$X_i = \kappa r_f \tag{1c}$$

$$X_o = D - X_i \tag{1d}$$

$$D = \kappa d \tag{1e}$$

$$X = \kappa r \tag{1f}$$

$$\kappa^2 = e^2 a(a+b) n_a^0 / \epsilon_0 \epsilon_{r,dl} k_B T = 2IF^2 / \epsilon_0 \epsilon_{r,dl} RT \tag{1g}$$

In the above definitions, X_{ca}, X_{an}, X_i, X_o, D, X, κ, r_{ca}, r_{an}, r_f, r, e, n_a^0, ϵ_0, $\epsilon_{r,dl}$, k_B, T, I, F, and R denote respectively the scaled

effective radius of cations (the scaled closest approach of cations to biocolloidal core), that of anions (the scaled closest approach of anions to biocolloidal core), that of fixed groups (the locations of inner plane of the fixed groups), the locations of the outer plane of the fixed groups, the scaled membrane thickness, the scaled distance measured from the core-membrane interface, the reciprocal Debye screening length, the effective radius of cations, that of anions, that of fixed groups, the distance, the elementary charge, the number concentration of cations in the bulk liquid phase, the permittivity of a vacuum, the relative permittivity of the electrical double layer, the Boltzmann constant, the absolute temperature, the ionic strength, the Faraday constant, and the gas constant. Without loss of generality, we assume that $r_f > r_{an} > r_{ca}$. The fixed groups are arranged so that the edge of the leftmost one is tangent to the core-membrane interface and that of the rightmost one is tangent to the membrane-liquid interface. Since the membrane phase is ion-penetrable, mobile ions may move across the membrane-liquid interface without structural obstruction. Referring to Figure 1b, the system is divided into 6 regions. I. $0 < X < X_{ca}$, which is the inner charge-free membrane. II. $X_{ca} < X < X_{an}$, which contains only cations in the inner uncharged membrane zone. III. $X_{an} < X < X_i$, which contains both cations and anions in the inner uncharged membrane zone. IV. $X_i < X < X_o$, which contains all charged species. V. $X_o < X < D$, which contains both cations and anions in the outer uncharged membrane zone. VI. $X > D$, which is the electrical double layer containing both cations and anions. Also, the region of $X < 0$ represents the charge-free biocolloidal core. Note that the fixed negative charge exists in region IV.

The total concentration of the nonuniformly distributed fixed groups in region IV, N_j, can be described by[22]

$$N_j = \begin{cases} \dfrac{2N_0[1+\alpha(X-X_i)]}{\alpha(X_o-X_i)+2} & j=1 \\ \dfrac{N_0\alpha(X_o-X_i)\{1+\exp[\alpha(X-X_i)]\}}{\exp[\alpha(X_o-X_i)]+\alpha(X_o-X_i)-1} & j=2 \end{cases} \quad (2)$$

where α, j and N_0 are, respectively, the nonuniform feature index characterizing the extent of nonuniformity of the fixed groups, the distribution type index for the fixed groups ($j = 1$ for linear distribution; $j = 2$ for exponential distribution) and the space-average concentration of the fixed groups. Note that as $\alpha \to 0$, N_j becomes a uniform distribution. If the fixed original functional groups, denoted by A, are capable of absorption of electrolyte cations, denoted by M, the equilibrium reaction in region IV can be expressed by $(A_nM_m)^{z+} \leftrightarrow nA^{c-} + mM^{a+}$, where n, m, z, and c denote respectively the number of the fixed original functional groups and that of cations involved in the formation of a cation-functional group complex, the valence of the complex, and that of the fixed original functional groups.[25] Since biocolloids are usually negatively charged in physiological conditions, c is a positive integer and $-ceN_jN_A$, N_A being the Avogadro number, becomes the concentration of the fixed charge without the cation-absorption reaction in region IV. Note that the stoichiometry for charge balance also leads to $z = ma - nc$. The equilibrium constant of the cation-absorption reaction, K, can be presented b

$$K = [A^{c-}]^n \cdot C_a^m / [(A_nM_m)^{z+}] \quad (3)$$

where

$$C_a = (n_a^0/N_A)\exp(-a\varphi) \quad (3a)$$

In these expressions, $[A^{c-}]$, C_a, and $[(A_nM_m)^{z+}]$ denote respectively the concentration of the fixed original functional groups, that of cations, and that of cation-functional group complexes, and $\varphi = e\phi/k_BT$ is the scaled electrostatic potential, where ϕ is the distribution of the electrostatic potential. Equation 3a represents the fact that the distribution of cations in region IV follows the Boltzmann distribution. From the conservation of the fixed groups at any position in region IV, we have

$$[A^{c-}] = N_j - n[(A_nM_m)^{z+}] \quad (4)$$

Substituting eqs 3a and 4 into eq 3 yields

$$\frac{[(A_nM_m)^{z+}]}{\{N_j - n[(A_nM_m)^{z+}]\}^n} = \frac{1}{K}\left(\frac{n_a^0}{N_A}\right)^m \exp(-am\varphi) \quad (5)$$

The scaled concentration of the fixed charge can be calculated by

$$P_j = N_A\{z[(A_nM_m)^{z+}] - c[A^{c-}]\}/an_a^0 = N_A\{(z+nc)[(A_nM_m)^{z+}] - cN_j\}/an_a^0 \quad (6)$$

The spatial variation in the scaled electrical potential can be described by the following Poisson equation:

$$\frac{d^2\varphi}{dX^2} = \epsilon_*'\frac{[-u\exp(-a\varphi) + v\exp(b\varphi) - wP_j]}{a+b} \quad (7)$$

where ϵ_*' is the ratio of the relative permittivity of the 6 regions to $\epsilon_{r,dl}$. For convenience, a vector for the presence/absence of fixed groups, anions, and cations, (w, v, u), is defined, and (w, v, u) = (0, 0, 0), (0, 0, 1), (0, 1, 1), (1, 1, 1), (0, 1, 1) or (0, 1, 1) represent, respectively, regions I through VI. The definitions of ϵ_*' for the 6 regions are respectively region I, $\epsilon_1' = \epsilon_{r,1}/\epsilon_{r,dl}$; region II, $\epsilon_2' = \epsilon_{r,2}/\epsilon_{r,dl}$; region III, $\epsilon_3' = \epsilon_{r,3}/\epsilon_{r,dl}$; regions IV and V, $\epsilon_m' = \epsilon_{r,m}/\epsilon_{r,dl}$; region VI, $\epsilon_6' = 1$. In these expressions, $\epsilon_{r,*}$, $*$ being 1, 2, 3, and m is the relative permittivity. The rationale behind spatial variations in permittivity categorized by the size of cations, anions, and fixed groups is the observations of the influence on permittivity by the presence of ionic species near the rigid interface. In addition, the dielectric property surrounding an interface is frequently characterized by the evidence that the farther the position measured from solid surfaces, the larger the permittivity at that position.[27] Since the external electric field is uniform and does not generate any contribution to the spatial concentration of ionic species, only the internal electrostatic effect is considered here. The boundary conditions associated with eq 7 are

$$\frac{d\varphi}{dX} \to 0 \text{ as } X \to 0 \text{ and } X \to \infty \quad (8a)$$

$$\epsilon_{r,1}\left(\frac{d\varphi}{dX}\right)_{X=X_{ca}^-} = \epsilon_{r,2}\left(\frac{d\varphi}{dX}\right)_{X=X_{ca}^+} \text{ and } \varphi(X_{ca}^-) = \varphi(X_{ca}^+) \quad (8b)$$

$$\epsilon_{r,2}\left(\frac{d\varphi}{dX}\right)_{X=X_{an}^-} = \epsilon_{r,3}\left(\frac{d\varphi}{dX}\right)_{X=X_{an}^+} \text{ and } \varphi(X_{an}^-) = \varphi(X_{an}^+) \quad (8c)$$

$$\epsilon_{r,3}\left(\frac{d\varphi}{dX}\right)_{X=X_i^-} = \epsilon_{r,m}\left(\frac{d\varphi}{dX}\right)_{X=X_i^+} \text{ and } \varphi(X_i^-) = \varphi(X_i^+) \quad (8d)$$

$$\left(\frac{d\varphi}{dX}\right)_{X=X_o^-} = \left(\frac{d\varphi}{dX}\right)_{X=X_o^+} \text{ and } \varphi(X_o^-) = \varphi(X_o^+) \quad (8e)$$

$$\epsilon_{r,m}\left(\frac{d\varphi}{dX}\right)_{X=D^-} = \epsilon_{r,dl}\left(\frac{d\varphi}{dX}\right)_{X=D^+} \text{ and } \varphi(D^-) = \varphi(D^+) \quad (8f)$$

Due to the uncharged biocolloidal core, the electrical field vanishes on the core-membrane interface along the r direction, which is described by eq 8a. Also, the electrostatic potential near the core−membrane interface is not equal to the Donnan potential because the membrane thickness and the electrical double layer are about the same order. Equations 8b through 8h express the continuities in the electrical field and the electrostatic potential between two neighbor regions.

For a steady flow of liquid in the direction parallel to the biocolloidal membrane, the scalar velocity distribution of the fluid in the radial direction, u, can be described by the following Navier−Stokes equation:

$$\eta\frac{d^2u}{dr^2} - ifu + \rho_{el}(r)E = 0, \quad 0 \le r \le \infty \quad (9)$$

where

$$\rho_{el} = aen_a^0[u\exp(-a\varphi) - \upsilon\exp(b\varphi)] \quad (9a)$$

In these expressions, η, i, f, and ρ_{el} denote respectively the liquid viscosity, the space-zone index for the resistance to fluid flow inside or outside the membrane phase ($i = 1$ for regions I through V; $i = 0$ for region VI), the friction coefficients of the biocolloidal membrane phase, and the space charge density of electrolyte ions. Recasting eq 9 into the scaled form becomes

$$\frac{d^2U}{dX^2} - i\lambda^2U = \hat{L}[-u\exp(-a\varphi) + \upsilon\exp(b\varphi)] \quad (10)$$

where the scaled quantities are

$$U = \frac{u}{U_0} \quad (10a)$$

$$\lambda^2 = \frac{f}{\eta\kappa^2} \quad (10b)$$

$$\hat{L} = \frac{\epsilon_0\epsilon_{r,dl}k_BTE}{(a+b)e\eta U_0} \quad (10c)$$

Since the friction of the membrane phase influences the fluid flow but the effect of applied electrical field on the fixed charge does not influence the fluid flow, no difference occurs among regions III through V in eq 10 provided φ is obtained. For convenience, the electrophoretic system can be equivalently described by the fact that the biocolloid is fixed in space and the fluid flow in the opposite direction of U_0. Thus, the boundary conditions associated with eq 10 can be assumed as

$$U \to 0 \text{ as } X \to 0 \quad (11a)$$

$$\left(\frac{dU}{dX}\right)_{X=X_{ca}^-} = \left(\frac{dU}{dX}\right)_{X=X_{ca}^+} \text{ and } U(X_{ca}^-) = U(X_{ca}^+) \quad (11b)$$

$$\left(\frac{dU}{dX}\right)_{X=X_{an}^-} = \left(\frac{dU}{dX}\right)_{X=X_{an}^+} \text{ and } U(X_{an}^-) = U(X_{an}^+) \quad (11c)$$

$$\left(\frac{dU}{dX}\right)_{X=D^-} = \left(\frac{dU}{dX}\right)_{X=D^-} \text{ and } U(D^-) = U(D^+) \quad (11d)$$

$$U \to -1 \text{ as } X \to \infty \quad (11e)$$

The core-membrane interface is selected as the nonslip plane, as indicated in eq 11a. Continuities in the velocity and the tangential component of the stress tensor between two adjacent regions are expressed in eqs 11b through 11d. Solving eq 7 subject to eqs 8a through 8f and eq 10 subject to eqs 11a through 11e simultaneously, the spatial variation in φ and U can be obtained. Since the scaled velocity approaches -1 at infinite distance from the biocolloid, the bulk-phase fluid velocity is $-U_0$ and the electrophoretic velocity can be evaluated. The electrophoretic mobility of a biocolloid can be obtained by

$$\mu = \frac{U_0}{E} \quad (12)$$

3. Results and Discussion

The electrophoretic behavior of a biocolloid covered with a cation-absorptive membrane is investigated through numerical simulation. Note that the thickness of the double layer is a function of ionic strength and dielectric constant of electrolyte solution, which are both fixed in the present study. Based on the double-layer thickness, the dimensionless distance is consistently scaled throughout the system. For biological entities, the friction coefficient of the membrane phase ranges normally from 10^{10} to 10^{13} Ns/m^4, $f = 10^{11}$ Ns/m^4 is selected as the typical condition for the evaluation of the electrophoretic mobility. Although absorption of cations by the fixed original functional groups, which possess negative charge, occurs, the membrane phase is negatively charged.

Figure 2 shows the scaled electrostatic potential distribution for various distributions of the fixed groups. For a fixed α value, the absolute value of φ near the uncharged core for an exponential distribution of the fixed groups is lower than that for a linear distribution of the fixed groups, as revealed in Figure 2. This is because assemblage of the fixed groups near the membrane−liquid interface for exponential distribution is stronger than that for the linear one. For a constant concentration of the fixed groups, a stronger assemblage of the fixed groups near the membrane−liquid interface leads to a smaller amount of the fixed groups near the membrane−core interface and a stronger rebound on the electrostatic potential from its local minimum, φ_m, against the fixed charge. Moreover, fluctuation of the electrostatic potential distribution in the system for $j = 2$ is stronger than that for $j = 1$, as shown in Figure 2. As suggested in Figure 2, the larger the α value, the lower the absolute value of φ_s for a fixed j. A large α value also represents strong assemblage of the fixed groups near the membrane−liquid interface. For the case of $j = 1$, φ_m reaches a constant as α increases. For the case of $j = 2$, $\alpha = 60$ means that the fixed groups are almost gathered together near the membrane−liquid interface, yielding strong shielding of the negative electricity by counterions around $X = D$. Thus, for $j = 2$, the absolute value of φ_m of $\alpha = 60$ is lower than that of $\alpha = 10$, as indicated in Figure 2. Since the cationic size exists, the electrostatic potential near the membrane−core interface is strongly compensated by counterions for the case of large α. Hence, the larger α, the larger the discrepancy between φ_m and φ_s for a fixed j, as implied in Figure 2.

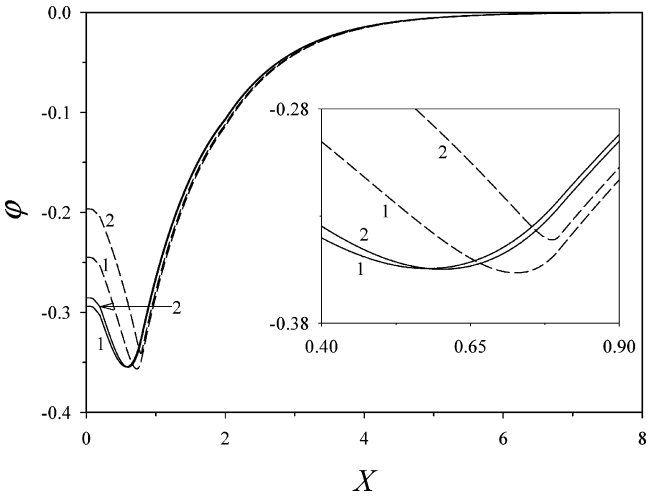

Figure 2. Scaled electrostatic potential distribution for various distributions of the fixed groups. Solid curves, $j = 1$, dashed curves, $j = 2$. Curves 1, $\alpha = 10$, 2, $\alpha = 60$. Key 1: $a = b = c = 1$, $n = m = 1$, $I = 10^{-3}$ mol/m^3, $D = 1$, $X_{ca} = 0.05$, $X_{an} = 0.1$, $X_i = 0.2$, $K = 6$ mol/m^3, $N_0 = 3$ mol/m^3, $\epsilon_{r,dl} = 78.5$, $\epsilon'_1 = 0.06$, $\epsilon'_2 = 0.2$, $\epsilon'_3 = 0.4$, $\epsilon'_m = 0.8$, and $T = 298.15$ K.

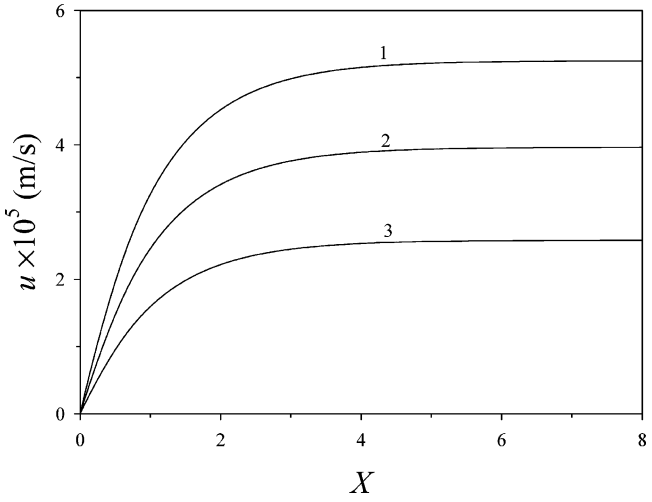

Figure 3. Fluid velocity distribution for various total concentrations of the fixed groups. Curve 1, $N_0 = 4$ mol/m^3; 2, $N_0 = 3$ mol/m^3; 3, $N_0 = 2$ mol/m^3. Key 1: same as in Figure 2 except N_0. Key 2: $j = 2$, $\alpha = 5$, $E = 800$ V/m, and $f = 1 \times 10^{11}$ Ns/m^4.

Fluid velocity distributions for various total concentrations of the fixed groups, cation-absorption equilibrium constants, and friction coefficients of biocolloidal membrane phase are presented in Figures 3−5, respectively. Note that a stationary biocolloid and uniform fluid velocity U_0 in bulk liquid phase are assumed according to the boundary conditions of the flow field in the present study. U_0 is equivalent to the electrophoretic velocity of a biocolloid. As revealed in Figure 3, the higher the total concentration of the fixed groups, the faster the fluid velocity and the larger U_0. Since the applied electrical field is constant, a high total concentration of the fixed groups results in a large absolute value of the electrophoretic mobility, $|\mu|$. This is because a high total concentration of the fixed groups represents high negative electricity in the biocolloidal membrane, rendering a faster biocolloidal velocity. As indicated in Figure 4, the larger the cation-absorption equilibrium constants, the faster the fluid velocity and the larger U_0. In the present study, the valence of the cation-functional group complex is zero, i.e., $z = ma - nc = 0$. Since a large cation-absorption equilibrium constant yields a small amount of uncharged cation-functional

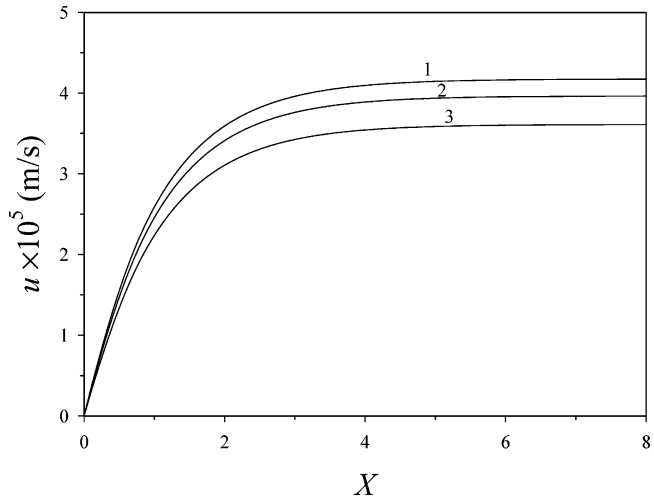

Figure 4. Fluid velocity distribution for various cation-absorption equilibrium constants. Curve 1, $K = 8$ mol/m^3; 2, $K = 6$ mol/m^3; 3, $K = 4$ mol/m^3. Key 1: same as in Figure 2 except K. Key 2: same as in Figure 3.

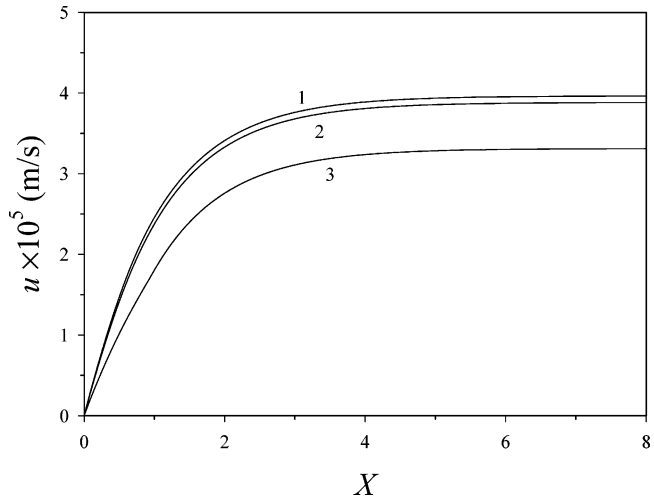

Figure 5. Fluid velocity distribution for various friction coefficients of the biocolloidal membrane phase. Curve 1, $f = 1 \times 10^{11}$ Ns/m^4; 2, $f = 1 \times 10^{12}$ Ns/m^4; 3, $f = 1 \times 10^{13}$ Ns/m^4. Key 1: same as in Figure 2. Key 2: same as in Figure 3 except f.

group complex and a large amount of dissociated complex, which is the negatively charged original functional groups, the absolute value of the electrostatic potential in the membrane phase becomes higher and the biocolloidal velocity is faster for larger cation-absorption equilibrium constants. Hence, it can be expected that the larger the cation-absorption equilibrium constant, the larger $|\mu|$. As suggested in Figure 5, a large friction coefficient of the biocolloidal membrane phase generates a slow fluid velocity. Since the friction coefficient means the resistance for fluid motion, a large friction coefficient of the biocolloidal membrane phase represents a high difficulty for fluid flow in the membrane phase, rendering a reduced U_0. As a result, a large friction coefficient of the biocolloidal membrane phase leads to small $|\mu|$.

Variation in the electrophoretic mobility as a function of nonuniform feature index is shown in Figure 6. As exhibited in the figure, the larger the nonuniform feature index, the larger $|\mu|$, in general. A large nonuniform feature index describes a biocolloidal membrane with high concentration of the fixed groups near the membrane−liquid interface, causing a large absolute value of φ_m, a large apparent electric field emanated from the membrane phase, high membrane electricity, and large

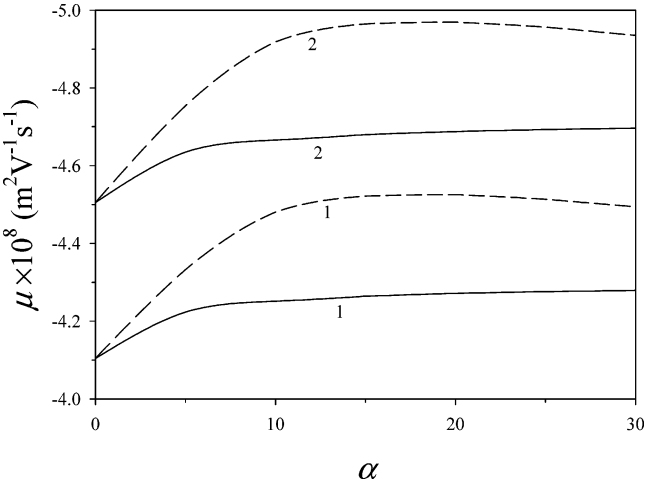

Figure 6. Variation in the electrophoretic mobility as a function of nonuniform feature index. Solid curves, $j = 1$, dashed curves, $j = 2$. Curves 1, $K = 4$ mol/m^3; 2, $K = 6$ mol/m^3. Key 1: same as in Figure 2 except *K*. Key 2: same as in Figure 3 except *j* and α.

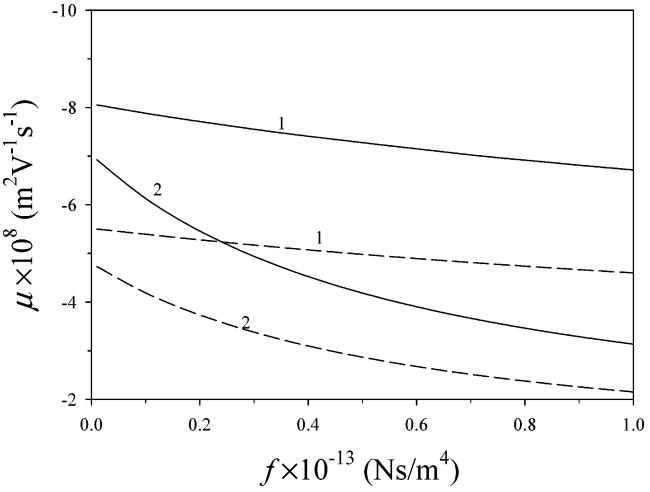

Figure 7. Variation in the electrophoretic mobility as a function of friction coefficient of the membrane phase. Solid curves, $N_0 \times (D - 0.4) = 5$ mol/m^3; dashed curves, $N_0 \times (D - 0.4) = 3.5$ mol/m^3. Curves 1, $D = 1$; 2, $D = 2$. Key 1: same as in Figure 2 except *D* and N_0. Key 2: same as in Figure 3 except *f*.

$|\mu|$. However, the influence of α on μ becomes weak if $\alpha > 5$ for $j = 1$ and $\alpha > 10$ for $j = 2$, as revealed in Figure 6. For $j = 2$, if α is larger than a critical value, $|\mu|$ decreases slightly with an increase of α. This is because condensed fixed groups near the membrane−liquid interface cause the shielding of electricity by counterions inside and outside membrane. Figure 6 also suggests that, for fixed α and *K*, $|\mu|$ of $j = 2$ be larger than that of $j = 1$, as expected. The above observations are consistent with the results of Figure 2. Moreover, the larger the cation-absorption equilibrium constant, the larger $|\mu|$, as indicated in Figure 6. This is consistent with the results of Figure 4.

Figure 7 presents the variation in the electrophoretic mobility as a function of friction coefficient of the membrane phase. Here, $N_0 \times (D - 0.4)$ is constant, i.e., the space-average total amount of the fixed groups in the membrane phase is fixed. Hence, a stronger electrostatic effect can be generated from a thinner membrane. As indicated in Figure 7, a larger $|\mu|$ results from a thinner membrane for a constant total amount of the fixed groups, as expected. For a fixed membrane thickness, the higher the total amount of the fixed groups and the smaller friction coefficient of the membrane phase, the larger $|\mu|$, as exhibited

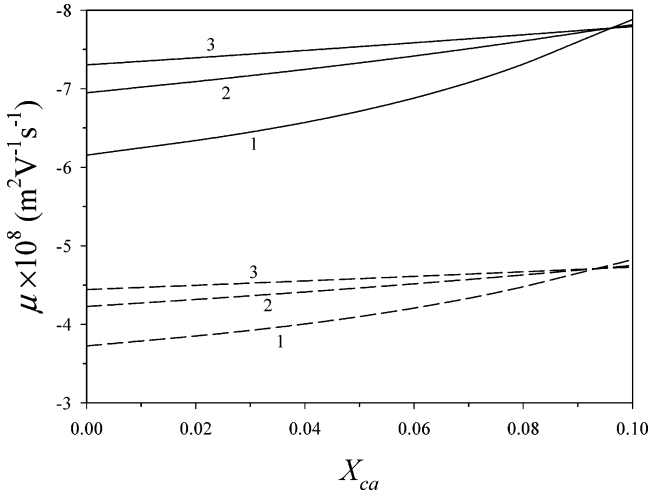

Figure 8. Variation in the electrophoretic mobility as a function of the scaled effective radius of cations. Solid curves, $m = 1$, dashed curves, $m = 2$. Curves 1, $\epsilon_2' = 0.06$; 2, $\epsilon_2' = 0.2$; 3, $\epsilon_2' = 0.4$. $N_0 = 4.5$ mol/m^3. Key 1: same as in Figure 2 except N_0, *m*, ϵ_2', and X_{ca}. Key 2: same as in Figure 3.

in Figure 7. These results are consistent with those presented in Figures 3 and 5.

Variation in the electrophoretic mobility as a function of the scaled effective radius of cations is shown in Figure 8. As presented in this figure, the larger the ratio of the dielectric constant of region II to the double-layer dielectric constant, the larger $|\mu|$ for a fixed effective radius of cations, in general. This is because a small dielectric constant of region II represents a strong nonpolar property of region II, where cations are repelled. Thus, more cations exist in region IV for a smaller ϵ_2' to neutralize the negative charge of the fixed original functional groups through absorption. Consequently, a small ϵ_2' generally yields low membrane electricity and small $|\mu|$. Also, $|\mu|$ increases with the effective radius of cations for a constant ϵ_2', as presented in Figure 8. Note that a larger effective radius of cations causes a smaller space of region II and φ_m is almost a constant as X_{ca} varies in the present study. Since rebound on the electrostatic potential occurs in region II, i.e., the absolute value of electrostatic potential increases with distance from biocolloidal core, a smaller space of region II, the slighter the potential rebound. Hence, a larger effective radius of cations yields a stronger electrostatic effect and larger $|\mu|$. This result is consistent with the tendency of interaction force investigated experimentally for various monovalent cations.[29] As suggested in Figure 8, the smaller the number of cations involved in the formation of a cation-functional group complex, the larger $|\mu|$. This is because a greater number of cations involved in the formation of a cation-functional group complex causes a stronger effect of electro-neutralization on the membrane fixed charge. For $0.09 < X_{ca} < 1$, an intersection of $\mu - Xc_a$ curves among various constant ϵ_2' values occurs, as shown in Figure 8. For an increase in the number of cations involved in the formation of a cation−functional group complex, X_{ca} value at the intersection decreases, implying some interference effects among the factors of X_{ca}, ϵ_2' and *m* on the electrophoretic mobility exist.

Variation in the electrophoretic mobility as a function of the scaled effective radius of anions is presented in Figure 9. As indicated in this figure, a larger ϵ_3' causes larger $|\mu|$ for a fixed effective radius of anions, in general. Since a large ϵ_3' attracts mobile counterions, a lesser amount of cations are absorbed in region IV and the negative membrane electricity becomes higher for a larger ϵ_3'. For a fixed ϵ_3' value, an increase in the effective

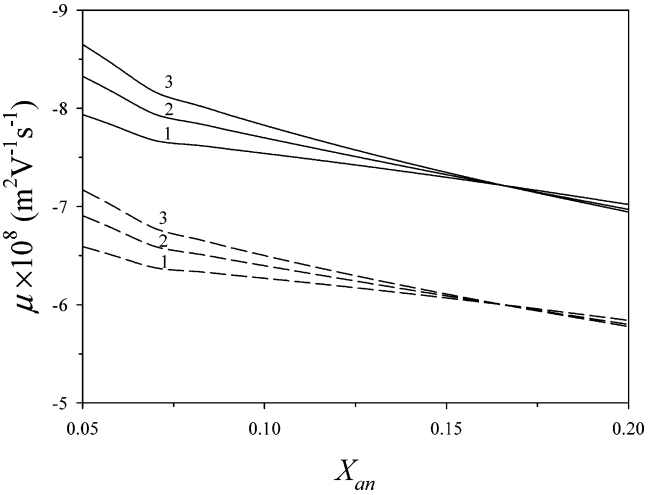

Figure 9. Variation in the electrophoretic mobility as a function of the scaled effective radius of anions. Solid curves, $f = 1 \times 10^{11}$ Ns/m^4; dashed curves, $f = 1 \times 10^{13}$ Ns/m^4. Curves 1, $\epsilon_3' = 0.2$; 2, $\epsilon_3' = 0.4$; 3, $\epsilon_3' = 0.8$. $N_0 = 4.5$ mol/m^3 and $K = 7$ mol/m^3. Key 1: same as in Figure 2 except N_0, K, ϵ_3', and X_{an}. Key 2: same as in Figure 3 except f.

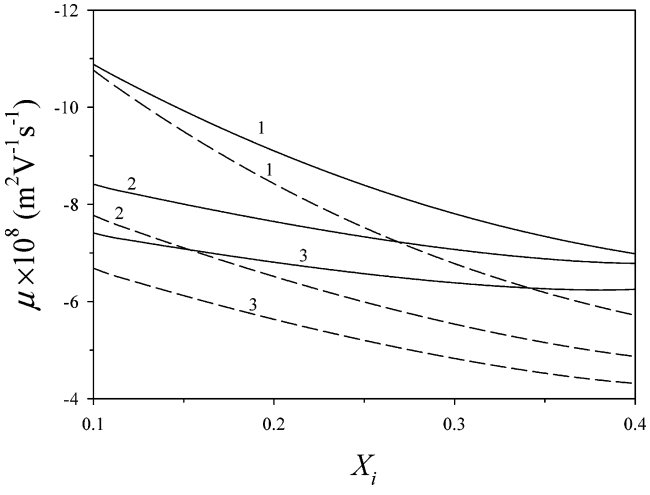

Figure 10. Variation in the electrophoretic mobility as a function of the scaled effective radius of fixed groups. Solid curves, $n = 1$; dashed curves, $n = 2$. Curves 1, $\epsilon_m' = 0.4$; 2, $\epsilon_m' = 0.8$; 3, $\epsilon_m' = 1$. $N_0 = 4.5$ mol/m^3 and $K = 7$ mol/m^3. Key 1: same as in Figure 2 except N_0, K, n, ϵ_m', and X_i. Key 2: same as in Figure 3.

radius of anions yields a decrease in $|\mu|$, as shown in Figure 9. This is because the absolute value of the electrostatic potential increases monotonically with distance from the membrane−core interface in regions II and III. Furthermore, the effect of increase in the absolute value of the electrostatic potential with distance in region II is stronger than that in region III, and larger anions yields a thicker region II and a thinner III. Note that φ_m is nearly fixed as X_{an} varies in the present study. Thus, a large effective size of anions leads to a reduction in the absolute value of the electrostatic potential in regions II and III, rendering a decrease in the electric effect on the electrophoretic mobility. As also revealed in Figure 9, the larger the friction coefficient of the membrane phase, the smaller $|\mu|$ for constant ϵ_3' and X_{an}. This is consistent with the results of Figure 5. As shown in Figure 9, an intersection of $\mu-X_{an}$ curves occurs among various constant ϵ_3' values for $0.15 < X_{an} < 0.175$, indicating the existence of some interference between the factors of X_{an} and ϵ_3' on the electrophoretic mobility. Also, X_{an} value at the intersection is almost independent of the friction coefficient of the membrane phase, as presented in Figure 9.

Figure 10 illustrates the variation in the electrophoretic mobility as a function of the scaled effective radius of fixed groups. As shown in Figure 10, a smaller ϵ_m' leads to larger $|\mu|$ for a fixed effective radius of fixed groups. This is because a smaller ϵ_m' represents more nonpolar regions IV and V and fewer cations penetrating into the membrane phase, yielding less absorption between cations and the fixed original functional groups and higher concentration of the fixed negative charge. A larger effective radius of fixed groups generates smaller $|\mu|$ for a constant ϵ_m' value, as indicated in Figure 10. Although a larger X_i causes a narrower space for region IV, over which the fixed groups are distributed, and yields a higher concentration of the original fixed charge, a larger X_i also results in wider spaces for regions III and V, where caions shelter the membrane from the negative electricity. Moreover, absorption of cations by the fixed original functional groups for a higher concentration of the original fixed charge becomes more severe than that for a lower one. As a result, the concentration of fixed negative charge is reduced for a large X_i. For a fixed ϵ_m' value, $|\mu|$ for the case of $n = 1$ is larger than that of $n = 2$, as suggested in Figure 10. Since a smaller number of the fixed original functional groups involved in the formation of a cation−functional group complex implies a lower reduction in the fixed negative charge by electroneutralization of cationic absorption, the smaller the n value, the higher the membrane electricity and the larger $|\mu|$.

The present model for cationic absorption by a cellular membrane can improve the agreement between experimental data and theoretical predictions. For example, the estimation of electrical property of articular chrondrocytes by the mobility detected from capillary electrolysis can be theoretically compared. Chrondrocytes require ionic nutrition and often interact with calcium, potassium, and sodium in normal situation and in biopathological state. Moreover, drug-delivery carriers, such as positively charged polybutylcyanoacrylate and negatively charged methyl methacrylate-sulfopropyl methacrylate nanoparticles (NPs),[30] can be absorbed by chrondrocytes for the purposes of pharmaceutical applications. Uptake of the biocompatible NPs by condrocytes during biomedical treatments may cause fluctuations in charge and the dielectric constant of the biological membrane. For ionic interaction and electrophoretic mobility in the above NPs-incorporated system, discrepancies between experimental results and theoretical values can be reduced by employing the present hypothesis.

4. Conclusions

In summary, the electrophoretic mobility of cation-absorptive biocolloids in an electrolyte solution was examined by taking the variation in dielectric constant of a biocolloidal membrane and sizes of ionic species into account. The simulated results indicate that strong membrane electricity yields a large absolute value of the electrophoretic mobility of biocolloids, $|\mu|$. Moreover, if the dominant parameters of the system for biocolloidal electrophoresis are categorized into the following 5 characteristics: cation absorption, functional-groups distribution, membrane, dielectric constant, and ionic size, it can be concluded that (1) for characteristics of cation absorption, a larger cation-absorption equilibrium constant and smaller numbers of cations and the fixed original functional groups involved in the formation of a cation-functional group complex lead to larger $|\mu|$; (2) for characteristics of functional-groups distribution, a nonlinear functional-groups distribution and a larger nonuniform feature index for functional-groups distribution lead to larger $|\mu|$; (3) for membrane characteristics, a higher

concentration of total fixed groups, a smaller friction coefficient of the biocolloidal membrane phase and a thinner membrane lead to larger $|\mu|$; (4) characteristics of dielectric constant, larger dielectric constants of region II and III and a smaller dielectric constant of regions IV and V, the main membrane phase, lead to larger $|\mu|$; (5) for characteristics of ionic size, larger cations and smaller anions and fixed groups lead to larger $|\mu|$. The simulated results also reveal the existence of some mutual interference in the electrophoretic mobility among effective size of cations, dielectric constant of region II, and numbers of cations involved in the formation of a cation−functional group complex, and between effective size of anions and dielectric constant of region III. The current cation-absorption model of biocolloids can be readily applied to study the relevant subjects in colloid and interfacial phenomena such as critical coagulation concentration and stability of a biocolloidal suspension and adsorption of biocolloids.

Acknowledgment. This work is supported by the National Science Council of the Republic of China.

References and Notes

(1) Sonohara, R.; Muramatsu, N.; Ohshima, H.; Kondo, T. *Biophys. Chem.* **1995**, *55*, 273.
(2) Mironov, S. L.; Dolgaya, E. V. *J. Membr. Biol.* **1985**, *86*, 197.
(3) Haydon, D. A.; Seaman, G. V. F. *Arch. Biochem. Biophys.* **1967**, *122*, 126.
(4) Tong, W.; Yeung, E. S. *J. Chromatogr. B* **1997**, *689*, 321.
(5) Torimura, M.; Ito, S.; Kano, K.; Ikeda, T.; Esaka, Y.; Ueda, T. *J. Chromatogr. B* **1999**, *721*, 31.
(6) Hunter, R. J. *Foundations of Colloid Science*; Oxford University Press: Oxford, 1989; Vol. 1.
(7) Levine, S.; Levine, M.; Sharp, K. A.; Brooks, D. E. *Biophys. J.* **1983**, *42*, 127.
(8) Ohshima, H.; Kondo, T. *J. Colloid Interface Sci.* **1987**, *116*, 305.
(9) Reiss, H.; Bassignana, I. C. *J. Membr. Sci.* **1982**, *11*, 219.
(10) Selvey, C.; Reiss, H. *J. Membr. Sci.* **1985**, *23*, 11.
(11) Kuo, Y. C.; Hsu, J. P. *J. Chem. Phys.* **1995**, *102*, 1806.
(12) Hsu, J. P.; Kuo, Y. C. *J. Membr. Sci.* **1995**, *108*, 107.
(13) Hsu, J. P.; Kuo, Y. C. *J. Chem. Phys.* **1995**, *103*, 465.
(14) Hsu, J. P.; Hsu, W. C.; Chang, Y. I. *Colloid Polym. Sci.* **1994**, *272*, 251.
(15) Tseng, S.; Lin, S. H.; Hsu, J. P. *Colloids Surf. B* **1999**, *13*, 227.
(16) Hsu, J. P.; Kuo, Y. C. *J. Chem. Phys.* **1999**, *111*, 4807.
(17) Kuo, Y. C.; Hsu, J. P. *J. Phys. Chem. B* **1999**, *103*, 9743.
(18) Kuo, Y. C.; Hsu, J. P. *Langmuir* **2000**, *16*, 6233.
(19) Kuo, Y. C.; Hsieh, M. Y.; Hsu, J. P. *Langmuir* **2002**, *18*, 2789.
(20) Huang, S. W.; Hsu, J. P.; Kuo, Y. C.; Tseng, S. *J. Phys. Chem. B* **2002**, *106*, 2117.
(21) Hsu, J. P.; Huang, S. W.; Kuo, Y. C.; Tseng, S. *J. Phys. Chem. B* **2002**, *106*, 4269.
(22) Kuo, Y. C. *Langmuir* **2003**, *19*, 5942.
(23) Kuo, Y. C. *J. Chem. Phys.* **2003**, *118*, 8023.
(24) Seaman, G. V. F.; Vassar, P. S.; Kendal, M. J. *Arch. Biochem. Biophys.* **1969**, *135*, 356.
(25) Kuo, Y. C. *J. Chem. Phys.* **2003**, *118*, 398.
(26) Zettlemoyer, A. C.; McCafferty, E. *Croat. Chem. Acta* **1973**, *45*, 173.
(27) Baldwin, J. L.; Dempsey, B. A. *Colloids Surf. A* **2001**, *177*, 111.
(28) Li, Y. H.; Zhao, K. S. *J. Colloid Interface Sci.* **2004**, *276*, 68.
(29) Colic, M.; Fishe, M. L.; Franks, G. V. *Langmuir* **1998**, *14*, 6107.
(30) Kuo, Y. C. *Int. J. Pharm.* **2005**, *290*, 161.